Multi-lambda hypernuclei and the equation of state of hypermatter

M. Rufa, J. Schaffner, J. Maruhn, H. Stöcker, and W. Greiner
Institut für Theoretische Physik der Johann Wolfgang Goethe Universität, Frankfurt, Germany

P.-G. Reinhard
Institut für Theoretische Physik der Universität Erlangen-Nürnberg, Erlangen, Germany
(Received 18 June 1990)

Within a relativistic mean-field theory (RMFT) experimental data on the single-particle spectra of lambda hypernuclei are well reproduced. It is shown that the coupling constants cannot be fixed unambiguously from the single-particle spectra. The stability and structure of multi-lambda hypernuclei is explored on the basis of the RMFT using the coupling constants as determined from the observed single lambda hypernuclear levels. It is predicted that multistrange nuclei exhibit an enhanced interaction radius, which further increases in the case of finite temperatures. We suggest that multi-lambda hypernuclei could be produced in high-energy heavy ions and observed in secondary noncharge-changing reactions. The equation of state of lambda matter and the possibility of pure lambda droplets are also discussed.

I. INTRODUCTION

Experiments at Brookhaven, CERN, and KEK (Refs. 1-7) have been used to investigate Λ hypernuclei, i.e., they allow the study of the effects of strangeness in nuclei. One of the prominent features is that the Λ is much less bound than nucleons. Several theoretical approaches have explained this effect.[7-10] In this paper we want to investigate *multi-*Λ hypernuclei[10] which might be produced in high-energy heavy-ion reactions. This is done within the framework of the relativistic mean-field theory, which has proved to give a very good description of normal nuclei.[11-15] Here we determine the Λ couplings in the (extended) relativistic mean-field model[10] by fitting the model spectra to the observed Λ-particle–nucleon-hole energy differences.[1-3] This model is then used to predict properties of multistrange hypernuclei, pure Λ droplets, and infinite Λ matter. We investigate binding energy, radius, and density as function of the successively added Λ's and the temperature. We are particularly interested in the enhanced interaction radii[10] which could explain the occurrence of anomalons in energetic heavy-ion reactions.[16,18,23]

The paper is organized as follows: In Sec. II we briefly present the model and determine the optimum Λ coupling constants. In Sec. III we discuss the new features of the suggested multi-Λ hypernuclei. In Sec. IV we discuss temperature effects. In Sec. V we investigate finite, pure Λ droplets and the equation of state of Λ matter. Our results are summarized in Sec. VI.

II. Λ HYPERNUCLEI

The relativistic mean-field model describes the nucleus as a system of Dirac nucleons coupled to explicit mesonic degrees of freedom. We start from the Lagrangian

$$\mathcal{L} = \mathcal{L}_{\text{Dirac}} + \mathcal{L}_\phi + \mathcal{L}_V + \mathcal{L}_R + \mathcal{L}_A , \tag{1}$$

with

$$
\begin{aligned}
\mathcal{L}_{\text{Dirac}} &= \bar{\psi}(i\gamma^\nu \partial_\nu - m_B)\psi + \bar{\psi}_\Lambda(i\gamma^\nu \partial_\nu - m_\Lambda)\psi_\Lambda , \\
\mathcal{L}_\phi &= \tfrac{1}{2}\partial_\nu \phi \partial^\nu \phi - \tfrac{1}{2}m_\sigma^2 \phi^2 - g_\sigma \phi \bar{\psi}\psi - g_{\sigma\Lambda}\phi \bar{\psi}_\Lambda \psi_\Lambda \\
&\quad - \tfrac{1}{3}b_2 \phi^3 - \tfrac{1}{4}b_3 \phi^4 , \\
\mathcal{L}_V &= -\tfrac{1}{4}G_{\mu\nu}G^{\mu\nu} + \tfrac{1}{2}m_\omega^2 V_\mu V^\mu - g_\omega V^\mu \bar{\psi}\gamma_\mu \psi \\
&\quad - g_{\omega\Lambda}V^\mu \bar{\psi}_\Lambda \gamma_\mu \psi_\Lambda , \\
\mathcal{L}_R &= -\tfrac{1}{4}\mathbf{B}_{\mu\nu}\cdot\mathbf{B}^{\mu\nu} + \tfrac{1}{2}m_\rho^2 \mathbf{R}_\mu \cdot \mathbf{R}^\mu - \tfrac{1}{2}g_\rho \mathbf{R}^\mu \cdot \bar{\psi}\tau\gamma_\mu \psi , \\
\mathcal{L}_A &= -\tfrac{1}{4}F_{\mu\nu}F^{\mu\nu} - \tfrac{1}{2}e A^\mu \bar{\psi}(1+\tau_0)\gamma_\mu \psi , \\
G^{\mu\nu} &= \partial^\mu V^\nu - \partial^\nu V^\mu , \quad F^{\mu\nu} = \cdots .
\end{aligned}
\tag{2}
$$

The notation follows the conventions of Refs. 14 and 15. Contributions from the Λ particles are added in $\mathcal{L}_{\text{Dirac}}$, $\mathcal{L}_\phi$, and $\mathcal{L}_V$, which introduce two new coupling parameters $g_{\sigma\Lambda}$ and $g_{\omega\Lambda}$. The Λ cannot contribute to $\mathcal{L}_R$ and $\mathcal{L}_A$ because it has isospin 0 and charge 0. The Lagrangian (1) is an effective Lagrangian for the relativistic mean-field theory where we treat the meson fields as classical c-number fields and where we neglect the contributions from the antiparticle states for nucleons and Λ's.

The coupled field equations are derived by standard field variation. We obtain, for stationary states,

$$(-\Delta+m_\sigma^2)\phi=-g_\sigma\rho_\sigma-g_{\sigma\Lambda}\rho_{\sigma\Lambda}-b_2\phi^2-b_3\phi^3 \ ,$$

$$(-\Delta+m_\omega^2)V_0=g_\omega\rho_0+g_{\omega\Lambda}\rho_0 \ ,$$

$$(-\Delta+m_\rho^2)R_{0,0}=\tfrac{1}{2}g_\rho\rho_{0,0} \ ,$$

$$-\Delta A_0=e\rho_{\mathrm{pr},0} \ ,$$

$$\varepsilon_\alpha\varphi_\alpha=\gamma_0\left[-i\gamma\cdot\nabla+m_B+g_\sigma\phi+g_\omega V_0\gamma_0+\frac{1}{2}g_\rho R_{0,0}\tau_0\gamma_0+eA_0\frac{1+\tau_{0\alpha}}{2}\gamma_0\right]\varphi_\alpha \ ,$$

$$\varepsilon_{\alpha\Lambda}\varphi_{\alpha\Lambda}=\gamma_0[-i\gamma\cdot\nabla+m_\Lambda+g_{\sigma\Lambda}\phi+g_{\omega\Lambda}V_0,V_0]\varphi_{\alpha\Lambda} \ ,$$

(3)

and the densities read

$$\rho_\sigma=\sum_{\alpha=1}^{\alpha=A}\omega_\alpha\overline{\varphi}_\alpha\varphi_\alpha \ , \quad \rho_{s\Lambda}=\sum_{\alpha=1}^{\alpha=A}\omega_\alpha\overline{\varphi}_{\alpha_\Lambda}\varphi_{\alpha_\Lambda} \ ,$$

$$\rho_0=\sum_{\alpha=1}^{\alpha=A}\omega_\alpha\overline{\varphi}_\alpha\gamma_0\varphi_\alpha \ , \quad \rho_{v\Lambda}=\sum_{\alpha=1}^{\alpha=A}\omega_\alpha\overline{\varphi}_{\alpha_\Lambda}\gamma_0\varphi_{\alpha_\Lambda} \ ,$$

$$\rho_{0,0}=\sum_{\alpha=1}^{\alpha=A}\omega_\alpha\overline{\varphi}_\alpha\gamma_0\tau_0\varphi_\alpha \ ,$$

$$\rho_{\mathrm{pr},0}=\sum_{\alpha=1}^{\alpha=A}\omega_\alpha\overline{\varphi}_\alpha\frac{1+\tau_{0\alpha}}{2}\gamma_0\varphi_\alpha \ . \tag{4}$$

Note that the sums run only over a few occupied shell-model states because effects of the Dirac sea are omitted (to be precise, they are assumed to be parametrized into the effective Lagrangian). Note furthermore that we have implemented occupation numbers ω_α which may be smaller than 1 in order to describe nonmagic nuclei with a partially filled valence shell. In practice, we compute the occupation numbers w_α by pairing with a constant gap $\Delta=11.2$ MeV$/\sqrt{A}$.[14] This yields

$$w_\alpha=\frac{1}{2}\left[1-\frac{\varepsilon_\alpha-\varepsilon_{\mathrm{Fermi}}}{[\varepsilon_\alpha-\varepsilon_{\mathrm{Fermi}})^2+\Delta^2]}\right]^{1/2} \ , \tag{5}$$

where the Fermi energy $\varepsilon_{\mathrm{Fermi}}$ is to be adjusted such that a given proton, neutron, or lambda number is reached by $\sum_\alpha\omega_\alpha$.

For spherical nuclei we have as further simplification radially symmetric fields ϕ, V_0, $R_{0,0}$ and A_0. The nucleon and Λ wave functions separate into spinor spherical harmonics and radial functions (for upper and lower Dirac components separately). The coupled equations for the spherical fields and radial wave functions are solved iteratively on a radial coordinate space grid. For details see Ref. 14.

The adjustment of the model parameters proceeds in two steps. First, the parameters of the model in the nucleon sector, g_σ, b_2, b_3, g_ω, g_ρ, m_σ, m_ω, and m_ρ, are fitted to the set of normal nucleus data,[14,15] namely, to the binding energy, radius, and surface thickness of the eight spherical nuclei ^{16}O, ^{40}Ca, ^{48}Ca, ^{58}Ni, ^{90}Zr, ^{116}Sn, ^{124}Sn, and ^{208}Pb. In addition, we have adjusted the same observables of ^{12}C (^{12}C will become important in considering the Λ spectra). We chose to stay with the standard parametrization [Eq. (1)] and to enable computation of ^{12}C by using a somewhat larger effective mass ($m^*/m=0.60$) at the cost of a slightly reduced precision of the fit. For the problems with ^{12}C and for a possible solution, see Ref. 19. The resulting parameters are shown in Table I. With the parameters of Table I we reproduce the ground-state properties of the light nuclei ^{12}C, ^{16}O, and ^{40}Ca with an average error of 0.3% for the radii, 0.9% for the energies, and 5% for the surfaces.

In a second step, we adjust the two additional parameters of the extended model, $g_{\sigma\Lambda}$ and $g_{\omega\Lambda}$. One usually considers the ratio $g_{\sigma\Lambda}/g_\sigma$ and $g_{\omega\Lambda}/g_\omega$, which expresses immediately the strength relative to the nucleon coupling. The quark model suggests furthermore that $g_{\sigma\Lambda}/g_\sigma=g_{\omega\Lambda}/g_\omega$, which has been chosen in a comparable work to be $\frac{1}{3}$.[9] However, that point of view may not carry through to the effective couplings of the mean-field model which incorporate also many-body effects. Nonetheless, it is useful to display relative strengths. In fact, we distinguish an average relative strength x and a difference of the relative strength, Δ, between scalar and vector coupling. They are defined as

$$g_{\sigma\Lambda}=g_\sigma(x+\tfrac{1}{2}\Delta) \ ,$$

$$g_{\omega\Lambda}=g_\omega(x-\tfrac{1}{2}\Delta) \ . \tag{6}$$

We adjust the two Λ couplings by a least-squares fit to

TABLE I. Nucleon parameters (bottom) and their dimensionless counterparts (top). The masses are given in MeV. The isovector vector mass is fixed to their one-boson exchange potential value $m_\rho=763$ MeV.

	C_σ^2	C_ω^2	C_ρ^2	B_2	B_3	m_σ	m_ω
Param. value	348.26	229.29	37.23	-0.22847×10^{-2}	-0.29151×10^{-2}	499.31	780.0

	g_σ	g_ω	g_ρ	b_2	b_3	m_σ	m_ω
Param. value	9.9339	12.592	4.9632	-10.6466	-28.3882	499.31	780.0

TABLE II. Parameter for the meson Λ couplings and their correlated errors expressed in three different forms.

	x	Δ	$g_{\sigma\Lambda}/g_\sigma$	$g_{\omega\Lambda}/g_\omega$	$C_{s\Lambda}^2$	$C_{\omega\Lambda}^2$
Full fit						
Param. value	0.473	-0.017	0.464	0.481	106.05	75.18
Corr. error	±0.285	±0.06	±0.255	±0.315	±114.74	±96.35
Restr. fit						
Param. value	0.390	0.00	0.390	0.390	74.86	49.28
Corr. error	±0.0163	±0.00	±0.0163	±0.0163	±6.26	±4.12

the experimental Λ-n spectra in ^{12}C, ^{16}O, and ^{40}Ca,[2-3] minimizing the squared deviation

$$\chi^2 = \sum_n \left[\frac{\mathscr{O}_n^{\text{expt}} - \mathscr{O}_n^{\text{theor}}}{\Delta\mathscr{O}_n} \right]^2 , \qquad (7)$$

with respect to the two Λ couplings $g_{\sigma\Lambda}$ and $g_{\omega\Lambda}$. The sum runs over the selected observables $\mathscr{O}_n$. $\Delta\mathscr{O}_n$ is the experimental uncertainty of the observable. Two cases have been considered: first, a full fit of both couplings, and second, a restricted fit under the hypothesis $g_{\sigma\Lambda}/g_\sigma = g_{\omega\Lambda}/g_\omega$, i.e., $\Delta=0$. The resulting parameters are given in Table II. The ten Λ-n energies which have been included in the fit are shown in Table III together with the fitted spectra. We assumed an average error of 2 MeV on the experimental spectra. We see that the fitted spectra approach the experimental data very well within this uncertainty. We see from Table II that both fits (full and restricted) give Λ couplings which are smaller than the nucleon couplings by a factor of about 0.4. This reduced Λ coupling is in accordance with all previous findings. The restricted fit reproduces the spectra already very well in view of the large experimental uncertainty. The full fit improves the reproduction a bit. Thus the as-

sumption of equal relative couplings ($\Delta=0$) may be sufficient. The results, however, do not prove this assumption because the error on Δ in the full fit is fairly large. In fact, the large errors on x and Δ show that the data are not precise enough yet to fix the full extended model. We will use both fits in the following investigations. The full fit with its larger uncertainties will produce the larger extrapolation errors (applying the rules of error propagation). These give the pessimistic view of the extrapolation power of the model, so to say, the conservative estimate. In Fig. 1(a) we show the s, p, d, and f single-particle energies of the Λ particle versus the mass of the nuclei employing the full fit, in comparison to the experimental data.[27] The case for the restricted fit is given in Fig. 1(b). It is quite remarkable that our restricted fit, which involves only one additional parameter, is nearly as good as the earlier nonrelativistic Skyrme model fits with three parameters.[28] In Fig. 2 we show the Λ potentials for both fits. The particle potential which is the sum of vector and scalar potentials has in both cases the same small depth of 30 MeV, whereas the scalar and vector potentials alone differ much more between the two fits. This means that the effective mass for the Λ particle is different for the two fits ($m_\Lambda^*/m_\Lambda \approx 0.84$ for the full

TABLE III. Λ-neutron-hole single-particle energy differences are all given in MeV. The experimental values are taken from Refs. 1 and 3; the errors vary between 1.5 and 2.5 MeV. For simplicity a typical error of $\Delta E = 2.0$ MeV is adopted. For the theoretical results also the deviation from the experimental values, $\delta E = E_{\text{expt}} - E_{\text{theor.}}$, is displayed in order to see better the features of the fits. In the last two columns we provide the average error and the mean-square error for both fits.

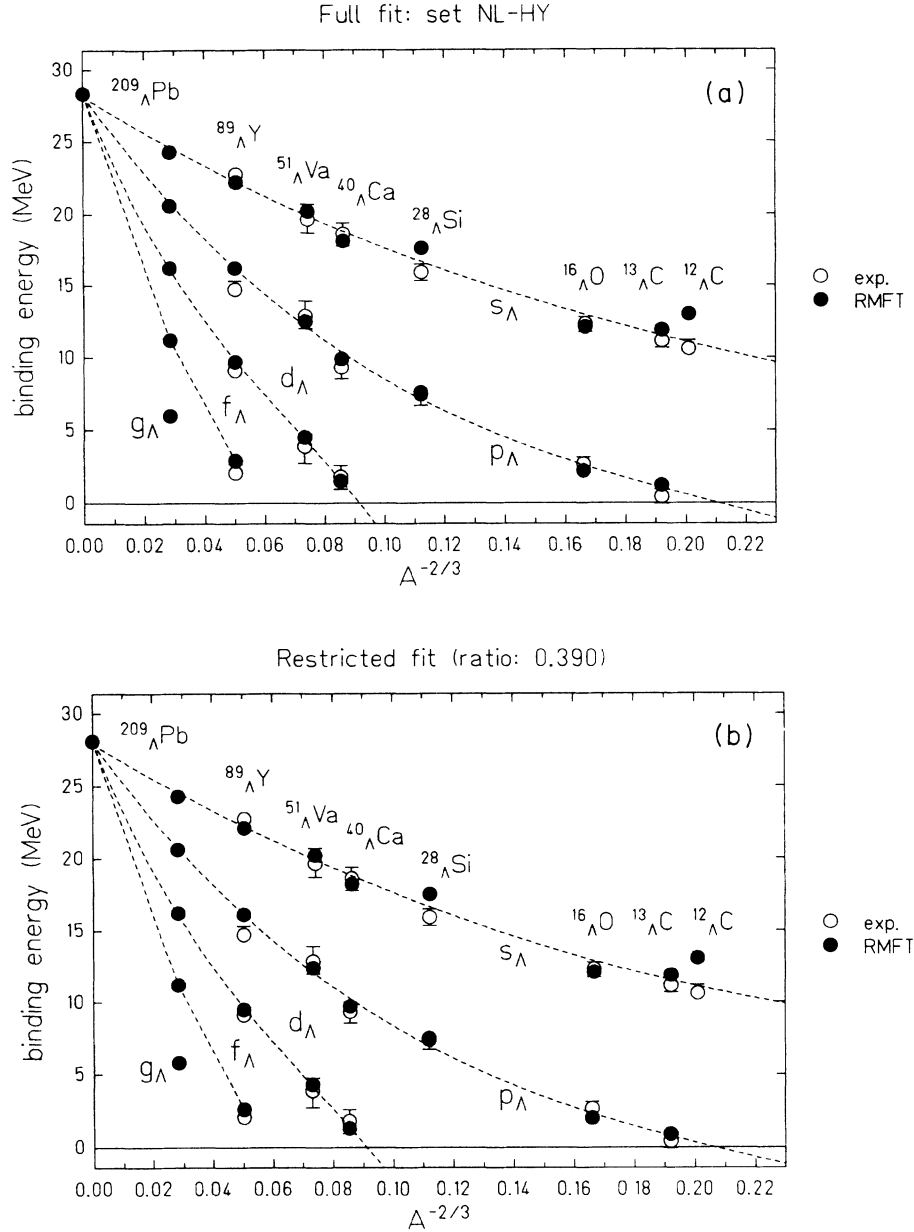|		Experimental		Full fit		Restr. fit	
Nucleus	Levels	E	ΔE	E	δE	E	δE
^{12}C	($1s_{1/2}$ Λ, $1p_{3/2}^{-1}$ hole)	6.72	2	5.02	1.70	4.78	1.94
	($1p_{3/2}$ Λ, $1p_{3/2}^{-1}$ hole)	18.48	2	17.21	1.27	17.44	0.49
^{16}O	($1p_{3/2}$ Λ, $1p_{3/2}^{-1}$ hole)	19.20	2	18.88	0.32	19.12	0.08
	($1p_{1/2}$ Λ, $1p_{1/2}^{-1}$ hole)	13.20	2	13.89	-0.69	13.95	-0.75
	($1s_{1/2}$ Λ, $1p_{3/2}^{-1}$ hole)	9.90	2	9.46	0.44	9.34	0.56
	($1s_{1/2}$ Λ, $1p_{1/2}^{-1}$ hole)	3.35	2	3.53	-0.18	3.41	-0.06
^{40}Ca	($1p_{1/2}$ Λ, $1d_{3/2}^{-1}$ hole)	5.79	2	7.40	-1.61	7.26	-1.47
	($1d_{3/2}$ Λ, $1d_{3/2}^{-1}$ hole)	14.47	2	15.48	-1.01	15.53	-1.06
	($1d_{5/2}$ Λ, $1d_{5/2}^{-1}$ hole)	19.35	2	20.71	-1.36	20.97	-1.62
	($1f_{7/2}$ Λ, $1d_{5/2}^{-1}$ hole)	28.24	2	27.14	1.10	27.41	0.83
$\overline{\delta E}$					-0.02		-1.06
$(\overline{\delta E^2})^{1/2}$					1.09		1.20

FIG. 1. (a) s_Λ, p_Λ, d_Λ, and f_Λ single-particle energies are plotted versus the atomic mass of the nuclei using the full fit in comparison to recent experimental data (Ref. 27) and are extrapolated to the hypernucleus $^{209}_\Lambda$Pb. (b) The same as in (a) for the restricted fit.

and ≈ 0.87 for the restricted fit). However, it is large as compared to the nucleon effective mass ($m^*/m \approx 0.6$) in any case.

The difference in the scalar and vector potentials, respectively, between the full and restricted fits, has apparently no influence on the single-particle spectra. In Table IV we extrapolate also to the spectra of some heavier nuclei up to the giant nucleus "double uranium," which is an object of interest for positron research.[20] The Λ spectra are compared with the neutron spectra. We see that both fits give the same results, showing the much smaller Λ binding and the reduced spin-orbit splitting.

III. MULTI-Λ HYPERNUCLEI

After we have fixed the model parameters by studying Λ hypernuclei, we will extrapolate the model to multi-Λ hypernuclei. The lambda single-particle potentials do not change dramatically as compared to the one-lambda case shown in Fig. 2. However, the density distributions of multihypernuclei do exhibit an interesting qualitative change: We observe the occurrence of a lambda halo when the neutrons in ^{16}O are successively replaced by more and more lambdas. In Fig. 3 we depict these density distributions of ^{16}O with zero, one, and seven lambdas.
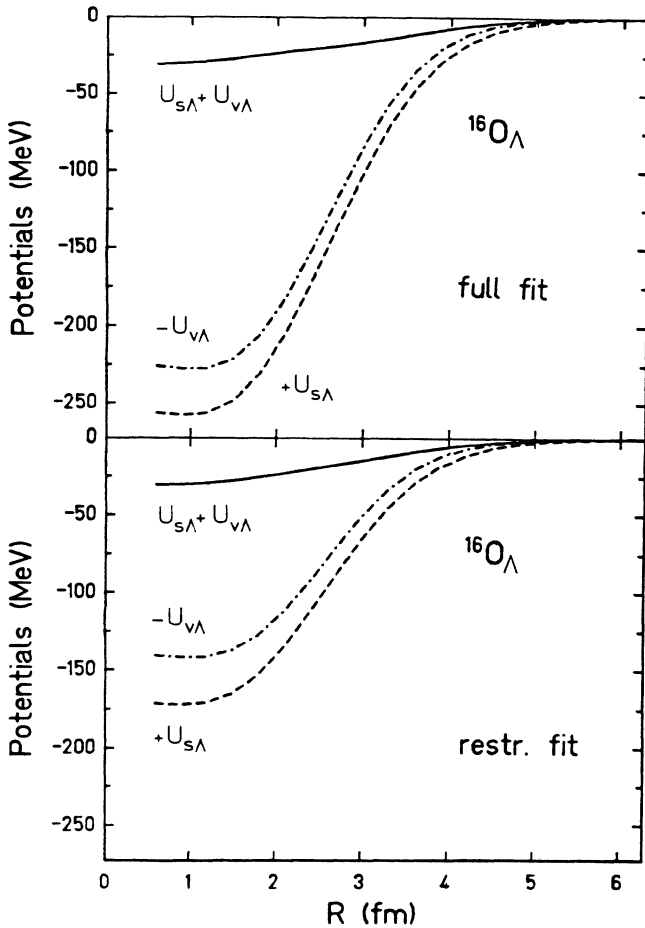
FIG. 2. Λ scalar and vector potentials and their sum are shown for both fits in $^{16}O_\Lambda$.

The total baryon densities and the lambda-vector density distribution given in Fig. 3(a) by the shaded areas turn out to be rather insensitive to the particular fitting procedure used (x stands for the restricted fit and x,Δ for the full fit). We want to point out that the Λ densities reach out much farther than the nucleon density: The size of the hypernuclei increases with increasing number of Λ's, although the baryon number is kept constant. The enhancement of the tail of the density distribution is best recognized in the logarithmic plot displayed in Fig. 3(b). Note the large (orders-of-magnitude) increase of the total baryon density at large radii as compared to normal nonstrange nuclei. Figure 3(c) gives the r^2-weighted densities. It shows that the interaction radii are dramatically changed when the more weakly bound Λ's are substituted for the neutrons.

These enhanced interaction radii offer a possibility to observe multi-Λ hypernuclei. They would behave analogously as the anomalous particles fragments (sometimes called "anomalons"):[16-18,23] These exotic multi-Λ hypernuclei would most probably have typical weak interaction lifetimes $\tau \sim 10^{-10}$ sec and exhibit unusually large interaction cross sections as compared to normal nuclei with the same Z. The latter is important, because their interactions with target nuclei would be insensitive to charge-changing reactions, which have been used in detector experiments as a counterproof to the emulsion results on anomalous particles fragments—the large interaction radius is due to the (neutral) Λ corona surrounding the charged core of the nucleus. This core can survive collisions, where only a few Λ's are stripped off. Indeed, a strong anomalous component has been observed for noncharge-changing reactions in Ref. 21. Therefore, it seems worthwhile to pursue the search for

TABLE IV. For the nuclei $^{12}C_\Lambda$, $^{16}O_\Lambda$, $^{40}Ca_\Lambda$, $^{48}Ca_\Lambda$, $^{208}Pb_\Lambda$, and the giant nucleus $^{476}G_\Lambda$, the lambda single-particle levels (given in MeV) are compared with the neutron levels.

| Level	^{12}C			^{16}O		
	Λ(FF)	Λ(RF)	N	Λ(FF)	Λ(RF)	N
$1d_{5/2}$						
$1d_{3/2}$						
$1p_{3/2}$	−0.70	−0.48	−17.92	−2.57	−2.34	−21.45
$1p_{1/2}$	−0.42	−0.44		−1.63	−1.57	−15.52
$1s_{1/2}$	−12.90	−13.13	−46.06	−12.00	−12.11	−40.65
	^{40}Ca			^{48}Ca		
$1d_{5/2}$	−3.76	−3.74	−22.85	−1.99	−1.74	−22.71
$1d_{3/2}$	−2.63	−2.82	−17.10	−0.88	−0.83	−16.36
$1p_{3/2}$	−11.61	−11.83	−37.70	−9.78	−9.75	−37.63
$1p_{1/2}$	−10.93	−11.30	−34.59	−8.96	−9.10	−33.42
$1s_{1/2}$	−19.43	−19.80	−52.74	−17.96	−18.17	−53.12
	^{208}Pb			^{476}G		
$1d_{5/2}$	−16.12	−16.29	−43.82	−19.83	−19.81	−48.16
$1d_{3/2}$	−15.78	−16.04	−42.47	−19.73	−19.73	−47.77
$1p_{3/2}$	−20.51	−20.68	−51.23	−22.45	−22.41	−52.49
$1p_{1/2}$	−20.38	−20.58	−50.67	−22.41	−22.37	−52.31
$1s_{1/2}$	−24.19	−24.35	−57.41	−24.63	−24.57	−56.13
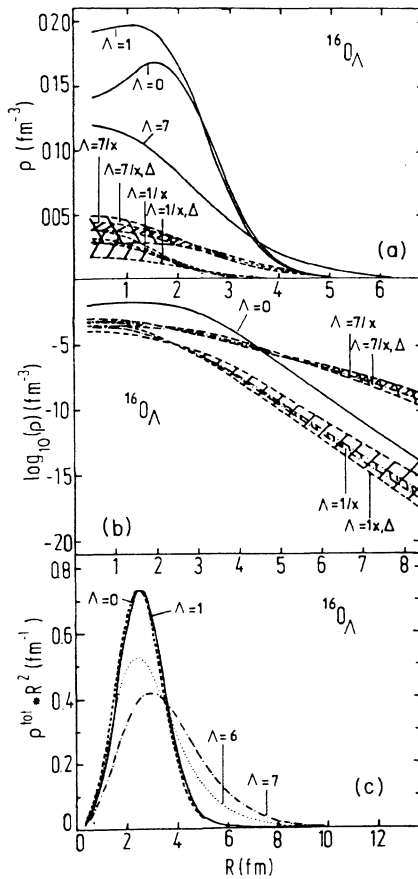
FIG. 3. (a) Shade areas give the Λ-vector density distributions $\rho_{\omega\Lambda}$ alone in $^{16}O_\Lambda$ for $\Lambda=1$ and 7 for both the restricted and full fit with their correlated error bands. The parameters varied are marked behind the slash. The total baryon densities $\rho_\omega^{tot}=\rho_\omega+\rho_{\omega\Lambda}$ (solid lines) with $\Lambda=0,1,7$ are shown for the full fit. (b) The vector density distributions of the normal nucleus (solid) and of the lambdas (dashed) are shown in a logarithmic scale. (c) The total baryon densities weighted with r^2 are shown for $\Lambda=0,1,6,7$ in $^{16}O_\Lambda$. These densities are plotted with the parameters of the full fit.

FIG. 4. (a) Total (R_{rms}^{tot}) and Λ (R_{rms}^Λ) root-mean-square radii are shown for the nucleus $^{16}O_\Lambda$ as a function of the substituted Λ number. (b) In $^{16}O_\Lambda$ the energy per nucleon is shown as a function of the substituted Λ's.

multistrange nuclei in experiments which look for secondary noncharge-changing reactions of high-energy heavy ions. The formation of multihypernuclei in high-energy heavy-ion collisions has been discussed in Ref. 22.

In Fig. 4(a) we show the rms radius and in Fig. 4(b) the binding energy for $^{16}O_{\Lambda=0,1,\ldots,7}$ as function of the replaced Λ's. The binding energy decreases and the Λ radius increases with increasing Λ content, whereas the total radius first decreases and turns back to an increase after more than 2 Λ's replaced. There occurs a dramatic increase of the radii at 7 Λ's. This can be explained as a Λ shell effect: The 7th Λ has to go into the $p_{1/2}$ shell, which is extremely weakly bound in the shallow Λ potential, replacing the neutron in the $1s_{1/2}$ shell. The 6th Λ replaces a p-shell neutron, for which the binding energy difference is much smaller. One should also note that— mostly due to the asymmetry energy (ρ-meson term)—the
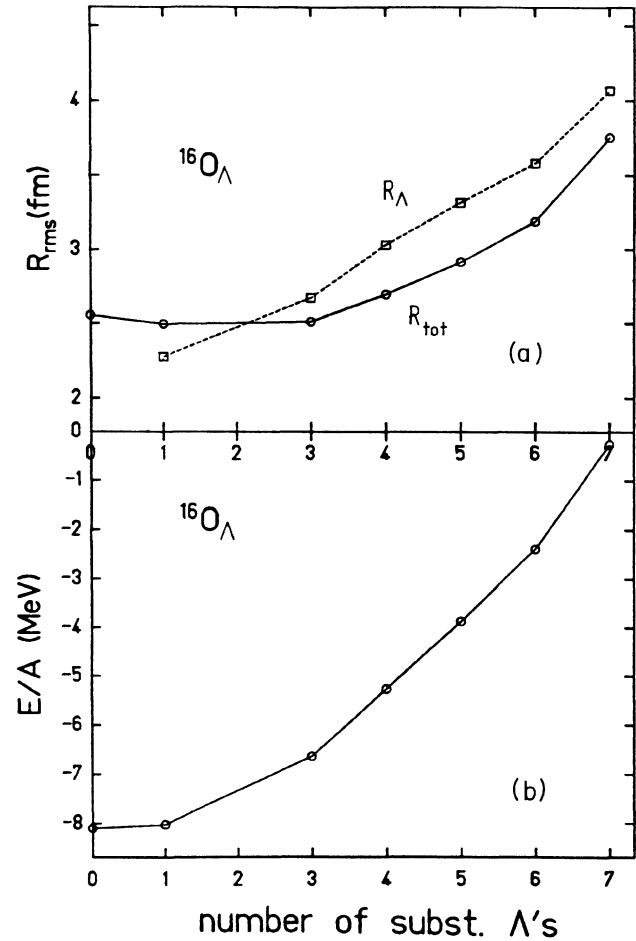
total binding energy is much less for this object (see Fig. 4).

A different behavior is observed for ^{48}Ca as the number of substituted Λ's increases (see Fig. 5) and ^{208}Pb (see Fig. 6). We see tighter binding when adding the first few Λ's. This is understandable by the Pauli principle. The first Λ's are taken from the last neutron valence states and packed into the lowest Λ states, which, of course, results in an enhanced binding and smaller radius. The trend is reversed if the available Λ states are less bound than the valence neutron states. This occurs after 8 Λ's for ^{48}Ca and after approximately 20 Λ's for ^{208}Pb. After that point the binding weakens and the radii grow quickly. There is a remarkable jump in the radii after 20 Λ's in ^{48}Ca and after 82 Λ's in ^{208}Pb. But the uppermost occupied Λ state reaches very soon after this jump the Λ continuum and the whole Λ nucleus becomes unstable with respect to particle emission.

IV. TEMPERATURE EFFECTS ON Λ HYPERNUCLEI

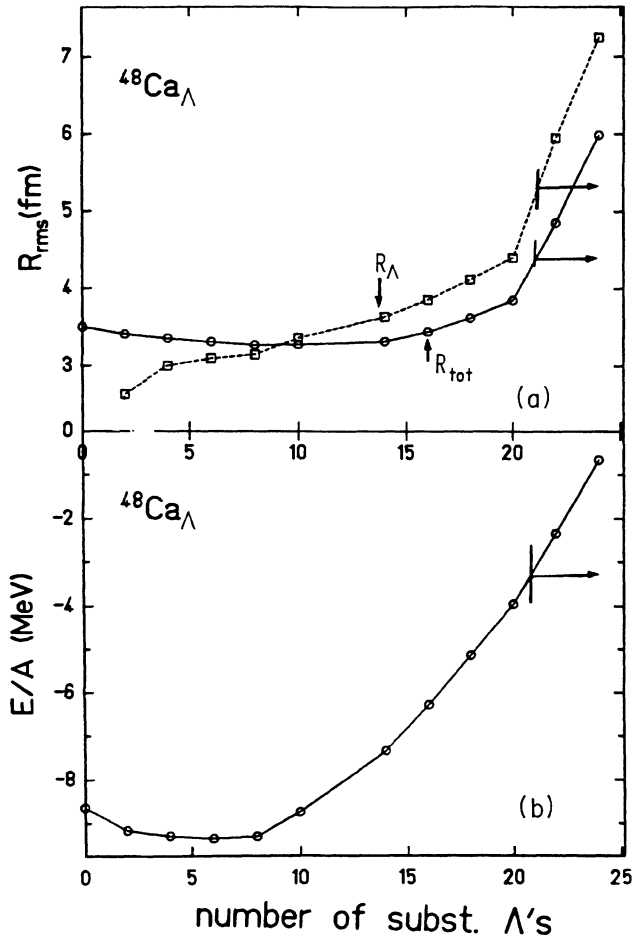In this section we investigate the influence of temperature on (multi-)Λ hypernuclei as compared to normal nu-

FIG. 5. (a) Total $(R_{\text{rms}}^{\text{tot}})$ and Λ $(R_{\text{rms}}^{\Lambda})$ root-mean-square radii are shown for the nucleus $^{48}\text{Ca}_\Lambda$ as a function of the substituted Λ number. (b) In $^{48}\text{Ca}_\Lambda$ the energy per nucleon is shown as a function of the substituted Λ's.
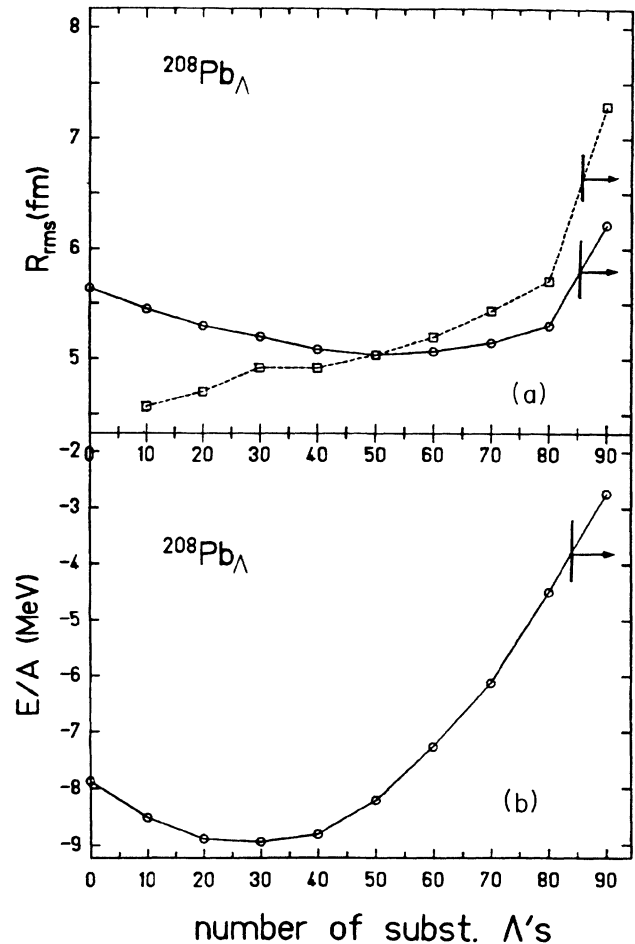
FIG. 6. (a) Total $(R_{\text{rms}}^{\text{tot}})$ and Λ $(R_{\text{rms}}^{\Lambda})$ root-mean-square radii are shown for the nucleus $^{208}\text{Pb}_\Lambda$ as a function of the substituted Λ number. (b) In $^{208}\text{Pb}_\Lambda$ the energy per nucleon is shown as a function of the substituted Λ's.

clei. To describe heated nuclei, we replace the pairing distribution (5) by the thermal Fermi distribution

$$\omega_\alpha = \left[1 + \exp\left[\frac{\varepsilon_\alpha - \varepsilon_{\text{Fermi}}}{T} \right] \right]^{-1}, \qquad (8)$$

where the Fermi energy $\varepsilon_{\text{Fermi}}$ is to be adjusted so that the desired particle number is reproduced in the average.

We show in Fig. 7 binding energy and radii as function of temperature for the nucleus ^{40}Ca with 0, 1, 8, or 12 substituted Λ's. The binding energies show the typical pattern for all cases. It starts with a nearly quadratic increase $E = a(kT)^2$. The coefficient a can be related to the average level density. We find $a = 4.4$ MeV for normal ^{40}Ca in the relativistic mean-field model, which compares very well with the $a = 4.3$ MeV which one obtains for nonrelativistic calculations using the Skyrme M^* force.[24] The level-density parameter becomes much larger if Λ's are added. We find $a = 8.3$ MeV for $\Lambda = 8$ and $a = 10$ MeV for $\Lambda = 12$. That is an effect of the much denser Λ spectrum due to the shallow Λ potential.

The radii show the more dramatic pattern. They increase strongly with temperature, in particular the Λ radii. We find that the Fermi distribution quickly places a substantial fraction of Λ's into the particle continuum. For the case $\Lambda = 8$, we have at $T = 5$ MeV already 25% of the Λ's in the continuum and for $\Lambda = 12$ at $T = 5$ MeV even 65%. A similar behavior is observed for other nuclei studied (^4He and ^{16}O). Thus we find that Λ hypernuclei are unstable against heating because most of the Λ's will evaporate quickly due to their shallow binding. Thus we conclude that multi-Λ hypernuclei can only survive if they are produced close to their ground state.

V. EQUATION OF STATE OF Λ MATTER AND Λ DROPLETS

The surprising stability of multi-Λ hypernuclei lead us to speculate about the possible existence of pure Λ matter or pure Λ droplets. The question of Λ matter (or nuclear matter with some Λ content) is also of interest for the properties of neutron stars and supernovae.[25]
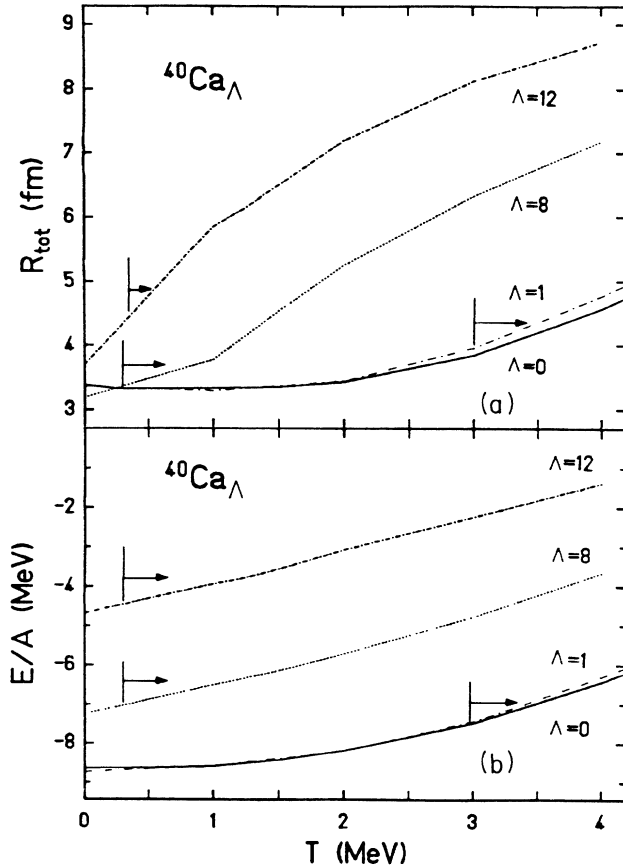
FIG. 7. (a) Behavior of the total and Λ radii is plotted for ^{40}Ca$_\Lambda$ with $\Lambda=0,1,8,12$ as a function of temperature and different numbers of Λ's substituted. (b) The binding energy per nucleon is shown for ^{40}Ca$_\Lambda$ as a function of temperature for these Λ numbers.

First, we investigate infinite hypermatter. We find that both parameter values obtained from the fits to single Λ hypernuclei, as given in Table II, cease to produce stable Λ matter. However, because there is a considerable uncertainty in the data, we have the freedom to vary these parameters at least within the error of the fit. It turns out that bound Λ matter can exist for quite a region in the plane of the two Λ coupling constants $C^2_{\sigma\Lambda}$ and $C^2_{\omega\Lambda}$. We have drawn the borderline between bound and unbound matter in Fig. 8 and indicate the half-plane of bound matter by an arrow. These borderlines are given for various strangeness fractions f of the matter, where f is the percentage of Λ's in the matter. In the parameter plane we also draw the ellipsis for a 1σ error on the parameters. It embraces all parameter combinations where the χ^2 according to Eq. (7) stays within $\chi^2 < \chi^2_{\min} + 1$. Each point within the error ellipsis is a parameter choice which is compatible with the experimental data on Λ spectra in light nuclei. The region of interest lies below the intersection of this error ellipsis with the half-planes of bound matter. We see that according to this analysis (meta-)stable Λ matter might very well exist. For admixtures f up to 50%, even the center point of the ellipsis
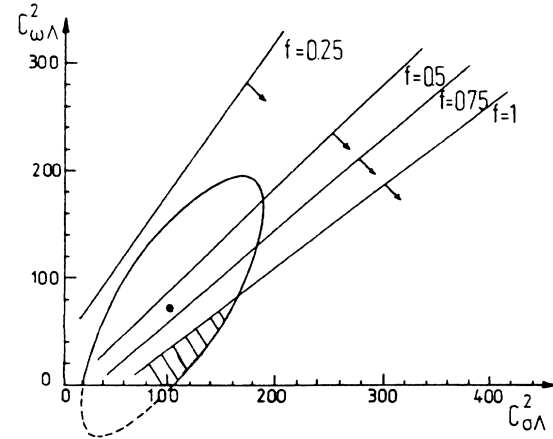

FIG. 8. Regions of bound and unbound Λ matter in the two-dimensional $C^2_{\sigma\Lambda}$—$C^2_{\omega\Lambda}$ plane. The borderline between bound and unbound matter is drawn for various ratios f of the Λ fraction in the mixed matter. The half-plane of bound matter is indicated by the arrow in each case. Furthermore, the error ellipsis of justifiable combinations of coupling parameters is drawn. The most interesting area is the intersection of the regions of bound pure Λ matter with the error ellipsis. It is dashed in the plot.

lies still in the half-plane of bound matter. The intersection of pure Λ matter with the error ellipsis is rather small, but it is not excluded within the large uncertainty of our present knowledge about Λ hypernuclei.

Let us now turn to possible existence of finite structures consisting of Λ only. We draw in Fig. 9 the half-planes, where bound Λ systems with $\Lambda=4$ and 16 can exist, together with the error ellipsis of the full fit. The dashed lines indicate extrapolations to parameter regions which lead to unstable calculations for the nonlinear model, but may be resolved by the functionals of Ref. 19. Again, only a small intersection region could possibly
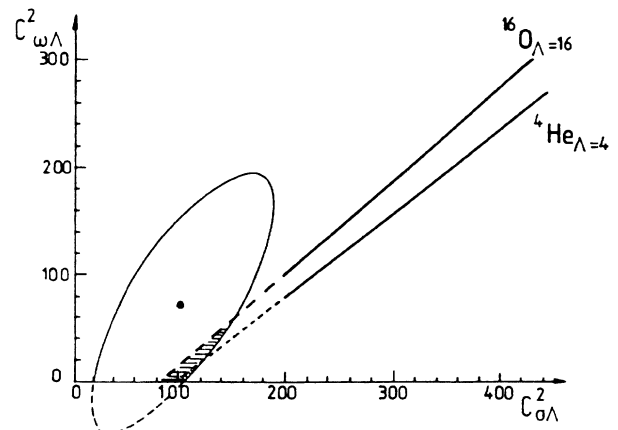

FIG. 9. Similar to Fig. 8, but for bound Λ droplets of 16 Λ's and 4 Λ's, respectively. The dashed lines indicate extrapolations to parameter regions which lead to instable calculations for the nonlinear model, but may perhaps be resolved by the functionals of Ref. 19.
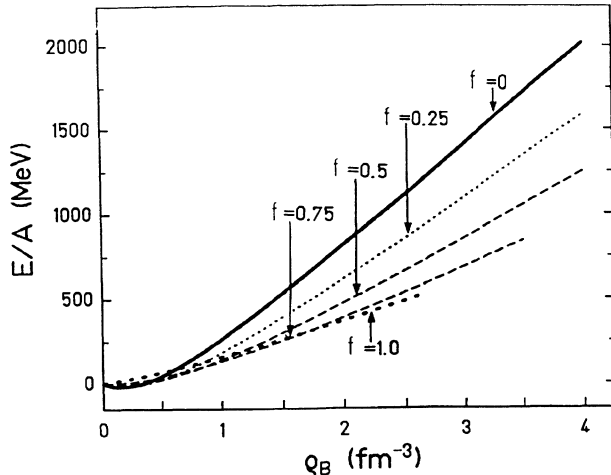
FIG. 10. Equations of state of Λ matter $(f=1)$, neutron matter $(f=0)$, and mixtures of lambda and neutron matter $(f=0.25-0.75)$.

lead to bound matter and be compatible with hypernucleus data at the same time. Whether Λ droplets do really exist can only be decided experimentally.

Also, other multistrange droplets, i.e., clusters of several Σ^-, Σ^+, and Σ^0, with or without Λ's, might be produced in heavy-ion collisions. Droplets of, e.g., $2\Sigma^-$, $2\Sigma^0$, 2Λ in their respective $1s$ states would be particularly easy to observe experimentally: They would have large mass, but negative charge, and so they could be easily separated in a spectrometer. These hyperon droplets should, however, not be misidentified as strangelets[26] which represent a droplet of deconfined u, d, and s quarks of the same strangeness content.

A question of interest in the physics of neutron stars is the effect of the Λ's on the equation of state for mixed neutron plus Λ matter. In Fig. 10 we show the energy per particle as function of the baryon density for pure neutron matter $(f=0)$, lambda matter $(f=1)$, and mixtures of neutron and lambda matter $(f=0.25, 0.5, \text{and} 0.75)$. We see that the Λ degree of freedom softens the equation of state substantially. This will have an effect on neutron stars where one has sufficient time to approach the strangeness-containing equilibrium. The times available for β equilibrium will be too short in energetic heavy-ion collisions to be achieved. However, the strange state of matter may contribute to the exit channel of a quark-gluon plasma with large strangeness.[26] In any case, the equation of state for strangeness-containing

matter will depend sensitively to the strength of the Λ coupling. One still needs more precise statements about this coupling to make more definite predictions at large densities.

VI. CONCLUSIONS

We have calculated single-particle energies, binding energies, radii, and density distributions of Λ hypernuclei in a relativistic mean-field model. The basis for these investigations was formed by a fit of the Λ coupling constants to hypernucleus data, whereas the nucleonic couplings have been fixed to various ground-state properties of eight spherical nuclei. The model can account for the observed spectra of Λ hypernuclei, but the coupling constants cannot unambiguously be determined from the single-particle levels. We find Λ coupling constants which are 0.4 of the coupling to the normal nucleus if $g_{\sigma\Lambda}/g_\sigma = g_{\omega\Lambda}/g_\omega$ is assumed. However, we find that this ratio is $\sim 0.5 \pm 0.3$ if both $g_{\sigma\Lambda}$ and $g_{\omega\Lambda}$ are varied. We have shown that the coupling constants could be determined by measuring the lambda density distribution.

We have studied the structure of multi-lambda hypernuclei, in particular their energy and radius as a function of the number of substituted lambdas. Their density distributions reach far beyond the interaction radii of normal nuclei. This gives rise to a behavior which is analogous to that of the anomalous particles fragments. But for higher temperatures and especially for higher Λ numbers, a large number of Λ particles are in the continuum. Thus we predict that hot multi-Λ hypernuclei evaporate before they could be observed.

We also investigated the equation of state of Λ matter and found bound lambda matter for model parameters compatible with data on finite hypernuclei.

It will be interesting to study single-particle properties of Σ hypernuclei in the present model, in particular the possible existence of negatively charged nuclei with positive baryon number. This would be easy to observe in spectrometer experiments and could constitute a viable doorway state to strangelets.

[1]B. Povh, Nucl. Phys. A335, 233 (1980).

[2]W. Brückner et al., Phys. Lett. 79B, 157 (1978).

[3]R. Bertini et al., Phys. Lett. 83B, 306 (1979).

[4]R. Bertini et al., Phys. Lett. 136B, 29 (1984); H. Piekarz et al., ibid. 110B, 428 (1982); R. Bertini et al., ibid. 158B, 19 (1985).

[5]W. Brückner, M. A. Faessler, K. Kilian, U. Lynen, B. Pietrzyk, B. Povh, H. G. Ritter, B. Schüerlein, H. Schröder, and A. H. Walenta, Phys. Lett. 55B, 107 (1975).

[6]M. May et al., Phys. Rev. Lett. 47, 1106 (1981); R. Chrien et

al., Phys. Lett. 89B, 31 (1979).

[7]For an excellent recent review on hypernuclei, see R. E. Chrien and C. B. Dover, Annu. Rev. Nucl. Part. Sci. 39, 113 (1989); earlier reviews include B. Povh, ibid. 28, 1 (1978); B. Povh, Prog. Part. Nucl. Phys. 5, 245 (1981); Proceedings of the International Symposium on Hypernuclear and Kaon Physics, Brookhaven, edited by R. E. Chrien [Nucl. Phys. A450, 1c (1986)]; Proceedings of the International Symposium on Hypernuclear and Kaon Physics, Bad Honnef, Germany, edited

by J. Speth [Nucl. Phys. **A479**, 1c (1988)]; see also E. H. Auerbach, A. J. Baltz, C. B. Dover, A. Gal, S. H. Kahana, L. Ludeking, and D. J. Millener, Ann. Phys. **148**, 381 (1983); E. H. Auerbach, A. J. Baltz, C. B. Dover, A. Gal, S. H. Kahana, L. Ludeking, and D. J. Millener, Phys. Rev. Lett. **47**, 1110 (1981); Y. Yamamoto, H. Bando, and J. Žofka, Prog. Theor. Phys. **80**, 757 (1988).

[8]R. Brockmann, and W. Weise, Phys. Lett. **69B**, 167 (1977); R. Brockmann and W. Weise, Nucl. Phys. **A355**, 365 (1981).

[9]J. Boguta and S. Bohrmann, Phys. Lett. **102B**, 93 (1981).

[10]M. Rufa, H. Stöcker, J. Maruhn, P.-G. Reinhard, and W. Greiner, J. Phys. G **13**, 143 (1987); J. Mares and J. Žofka, Z. Phys. A **333**, 209 (1989).

[11]B. D. Serot, and J. D. Walecka, Adv. Nucl. Phys. **15**, 1 (1986).

[12]A. Bouyssy, S. Marcos, and Pham van Thieu, Nucl. Phys. **A422**, 541 (1984); A. Bouyssy, *ibid.* **A290**, 324 (1977).

[13]J. Boguta and J. R. Bodmer, Nucl. Phys. **A292**, 414 (1977).

[14]P.-G. Reinhard, M. Rufa, J. Maruhn, W. Greiner, and J. Friedrich, Z. Phys. A **323**, 13 (1986).

[15]M. Rufa, J. Maruhn, W. Griner, P.-G. Reinhard, and M. Strayer, Phys. Rev. C **5**, 390 (1988).

[16]E. M. Friedlander, R. W. Gimpel, H. H. Heckmann, Y. J. Karant, B. Judek, and E. Ganssauge, Phys. Rev. Lett. **45**, 1084 (1980).

[17]G. Dersch, R. Beckmann, G. Feige, T. Lund, P. Vater, R. Brandt, E. Ganssauge, K. Aleklett, E. M. Friedlander, P. L. McGaughey, G. T. Seaborg, W. Loveland, J. Hermann, and N. T. Porile, Phys. Rev. Lett. **55**, 1176 (1985).

[18]J. D. Stevenson, J. A. Musser, and S. W. Barwick, Phys. Rev. Lett. **52**, 515 (1984).

[19]P.-G. Reinhard, Z. Phys. A **329**, 257 (1988).

[20]J. Reinhard, U. Müller, B. Müller, and W. Greiner, Z. Phys. A **303**, 173 (1981).

[21]A. P. Gasparian and N. Grigalashvili, Z. Phys. A **320**, 459 (1985).

[22]M. Sano, in *The Nuclear Equation of State,* Vol. 216 of *NATO Advanced Study Institute, Series B: Physics,* edited by W. Greiner and H. Stöcker (Plenum, New York, 1950), p. 231; M. Wakai, H. Bando, and M. Sano, Phys. Rev. C **38**, 748 (1988); H. Bando, Nuovo Cimento **A102**, 627 (1989).

[23]B. F. Bayman and Y. C. Tang, Phys. Rep. **147**, 155 (1987).

[24]W. Besold, P.-G. Reinhard, and C. Toepffer, Nucl. Phys. **A431**, 1 (1984).

[25]N. K. Glendenning, Z. Phys. A **326**, 57 (1987).

[26]A. R. Bodmer, Phys. Rev. D **4**, 1601 (1971); S. A. Chin and A. K. Kerman, Phys. Rev. Lett. **43**, 1292 (1979); E. Witten, Phys. Rev. D **30**, 272 (1984); E. Farhi and R. L. Jaffe, *ibid.* **30**, 2379 (1984); C. Greiner, P. Koch, and H. Stöcker, Phys. Rev. Lett. **58**, 1825 (1987); C. Greiner, D. H. Rischke, P. Koch, and H. Stöcker, Phys. Rev. D **38**, 2797 (1988).

[27]R. E. Chrien, Nucl. Phys. **A478**, 705c (1988); R. E. Chrien, Nuovo Cimento A **102**, 727 (1989).

[28]D. J. Millener, C. B. Dover, and A. Gal, Phys. Rev. C **38**, 2700 (1988).